Comparative analytical analysis of various configurations of nanoscaled dielectric-modulated double gate MOSFET based biosensors

B. BUVANESWARI[a,*], N. B. BALAMURUGAN[b]
[a]*Department of Computer Science and Engineering, K.L.N. College of Engineering, Madurai, Tamilnadu, India-630612*
[b]*Department of Electronics and Communication Engineering, Thiyagarajar College of Engineering, Madurai, Tamilnadu, India-625015*

In this paper, an analytical model for DG MOSFET based biosensor has been developed by applying Dielectric Modulation (DM) technique. This paper dealt with three types of DG MOSFET structures. These structures are classified with respect to the location of a uncovered region, which is acting as a door for the biomolecules. The uncovered region is called as a nanocavity region, that is formed by etching the gate oxide layer. In the first configuration, biomolecules are immobilized near the source. In the second configuration, the immobilization has been done near the drain. In the next configuration, the biomolecules are interacting through the vicinity of both the source and drain regions. This paper summarizes the performance metric such as sensitivity of the various biosensors and the metrics have been compared. The short channel effects of various configurations are analyzed and their mitigation level is compared , in order to put forward a optimum device structure in a nanoscaled limit.

(Received March 14, 2018; accepted October 10, 2018)

Keywords: Poisson 's equation, Parabolic approximation, Short channel effects, Biosensor

1. Introduction

Metal Oxide Semiconductor Field Effect Transistor (MOSFET) based biosensors have tremendously increased because of the unlimited benefits of Complementary Metal Oxide Semiconductor (CMOS) technology. Usual biomedical laboratories had been established with a costly medical equipments which consumes a lot of power. Moore's law is the observation that the number of transistors in a dense integrated circuit doubles approximately every two years [1]. The aggressive scaling of CMOS technology solves the problem of cost, power as it can be designed as a handheld or inside the pocket gadget . A biosensor is defined as a compact analytical device incorporating a biological sensing element integrated within a physico-chemical transducer whose aim is to produce optical or electronic signals proportional to the concentration of an analyte in a sample. In recent times, the investigations on Field Effect Transistor (FETs) based biosensors have been increasing drastically. They are the prospective candidate for the implementation of the label free biosensors. As the characteristics of biosensors are based on the physics related process, the inexpensive and efficient virtual experimentation is possible with the partial differential equations. Recently developed mathematical models of FET-based bio sensors are based on the surface potential model ,where the potential is derived from the Poisson's equation with suitable boundaries [2-5]. For accurate sensing of bio/chemical molecules, the thickness of the channel should be similarto the impact dimension of a biomolecule. The behaviour of the channel is totally different as soon as the channel region becomes the same order of magnitude as the depletion layer width of source and drain. The continuous scaling leads to the following short channel effects which are harmfully affect the device performance. The performance of a extremely scaled FET will be enhanced by the novel MOSFET structures like MultiGate (MuG) MOSFETs, halo Doping, high-k dielectric, strain engineering. In the MuG MOSFET structures, gate has the overall control on thinner silicon channel and the influence of drain will be suppressed. An alternative channel material will improve the transport properties than Si [6]. Label-free and real-time recognition of ions and charged molecules had been accomplished with the Field effect transistors (FETs) based devices. Bergveld reported a first Ion-sensitive FETs (ISFETs) [7]. In ISFETs , biomolecules were landing on the insulator region through an aqueous solution. The feature of ion and its concentration caused a noticeable change in the response of the ISFETs. Subsequently, Silicon MOSFET based biosensors were developed to detect the bio/chemical species. Two types of biomolecules were discussed namely fixed charge biomolecules and neutral biomolecules. The biomolecules are characterized with the fixed positive/negative charge densities and with the dielectric constant values. The biomolecules are immobilized on the top surface of oxide region. It creates a measurable change in the electrical characteristics of the biosensors. This rate of change was considered as a

sensing metric of MOSFET based biosensors. Following the reports , many types of FETs were developed for detecting bacteria, protein and ions. They are not limited to Silicon MOSFETs. They were also fabricated with nanomaterials like Graphene , Carbon nanotubes due to their biocompatibility. Also the next generation MOSFET biosensors will be designed for the ultra sensitive detection with Molybdenum Disulfide (MoS_2) layers [8]. Since the Lab-on-a-chip technology is aiming for a portable or handheld devices for the synthesis and analysis process of bio/chemical species and MOSFETs have the advantage of being able to be highly integrated on a single chip, MOSFET based biosensors have been investigated as the promising candidate in the biosensor fabrication. Since MOSFETs are shrinking to reach Giga-Scale Integration (GSI), QMEs need to be considered in MOSFET design and modeling. The mixture of the ultra-thin oxide layer and the heavily doped channel invalidate an accurate modeling of MOSFETs solely by classical physics. So the QMEs of the device must be taken into account. The tunnelling , energy quantization, and gate capacitance degradation are the very important QMEs [9-10]. Reports have shown better scalability of multi-gate MOSFETs over bulk MOSFETs [11-12]. Recently, conventional MOSFET biosensor is embedded with a nanocavity through which the immobilization of the biomolecules is accomplished. This nanogap embedded FET is also named as a dielectric-modulated FET (DMFET) . The nanogap was created by carving some parts of the sacrificial layer pre-existing between the gate and gate oxide. Latest reports acknowledges the very high sensitivity with the MOS_2 based label-free biosensors. Even though lots of research going on to find a hope, delayed disease diagnosis is still a major reason of death in today‘s world. It has been reported that timely detection of biomarkers can pave the way for early detection and successful treatments. For this reason, various biosensing mechanisms can be used to convert the signal coming from the recognition elements on the biosensor surface to the digital domain for signal processing. The performance metrics such as potential, threshold voltage, sensitivity of a DG MOSFET biosensor have been analyzed with and without biomolecules. The rate of change of threshold voltage has been considered as the sensing metric for detection of biomolecules under dry environment condition. The rest of the paper is organized as follows. In section II, the device structure and its working principle are presented. In Section III, the analytical modeling of device parameters has been discussed. Descriptions of the results have been shown in Section IV. The conclusion is presented in Section V.

1.1. Application of MOSFET as a biosensor

Among various types of biosensors, the MOSFET based biosensors became more popular because of the benefits like movable instrumentation, sensitive measurement , little amount of sample and speed. Bio-FETs for an assay of pencilin is the first FET based biosensor that was reported by caras and Janata[13]. The FET based DNA-Protein interaction was reported by Han et al[14]. An accurate dielectric modulation effect due to the charged biomolecules have been discussed by souteyrand et al [15]. In this the double stranded DNA (ds-DNA) is assumed. In the recent reports, a hand held biosensor is discussed with the extended gate electrical double layer FET technology[16]. It supports the Direct detection of protein biomarker in whole blood without extensive pre-treatments. An early detection of dengue virus non structural protein is reported by Nirton C. S. Vieira et al. [17]. Implantable MOSFET dosimeter was discussed to maintain a radiation dose for the cancer patients[18].

2. Device architecture

Different structures of Dielectric modulated DG MOSFET based biosensor are depicted in Fig. 1, Fig. 2, Fig. 3. Here, 100 nm channel length (L) is used. In Fig. 1, nanocavity with the length of 50 nm (L_1) is formed near the source. In Fig. 2, nanocavity with the length of 50 nm (L_2) is formed near the drain.In Fig. 3, nanocavity is formed near the source with the length of 25 nm (L_1) and near the drain with the length of 25 nm (L_3). Nanocavity regions are behaving like a sensing sites for the label free detection of biomolecules. Without the biomolecules, the cavity is assumed to be filled with air. The presence of the charged biomolecules like DNA, Protein etc., are altering the flat band voltage of the nanocavity region. The neutral biomolecules like glucose can modify the capacitance, dielectric constant of the nanocavity region. Due to these dielectric modulation effects, the device undergoes a threshold voltage shift. This shift is termed as a sensitivity of the device.

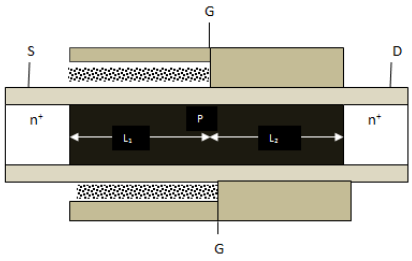

Fig. 1. Schematic of DG MOSFET based biosensor with the nanocavity formed near the source (first configuration)

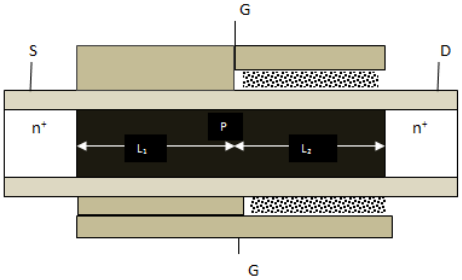

Fig. 2. Schematic of DG MOSFET based biosensor with the nanocavity formed near the drain (second configuration)

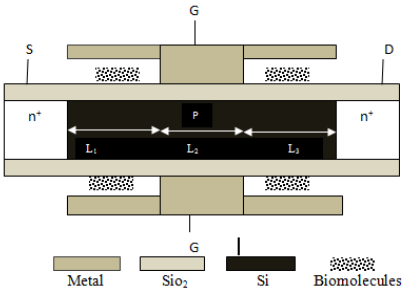

Fig. 3. Schematic of DG MOSFET based biosensor with the nanocavity formed near the drain and drain (third configuration)

3. Potential modeling

To model the proposed biosensor, two dimensional Poisson's equation is preferred. The device physics in the nanoscale region can be accurately described with the 2D Poisson equation.

4. Surface potential modeling

A 2D Poisson's equation with uniform doping is used to describe the potential field caused by the charge. The potential distribution in the silicon film is denoted as:

$$\frac{\partial \phi(x,y)}{\partial x^2}+\frac{\partial \phi(x,y)}{\partial y^2}=\frac{qN_A}{\varepsilon_{si}} \tag{1}$$

As the potential distribution is along with the y-direction, a parabolic approximation is applied to solve the Poisson's equation. A simple parabolic approximation is as follows:

$$\phi(x,y)=\phi_s(x)+a_1(x)y+a_2(x)y^2 \;;0\le x\le L,0\le y\le t_{si} \tag{2}$$

For the first configuration (cavity near Source) and second configuration (cavity near drain) to acquire an analytical expression of potential distribution , the channel is divided in to two regions and for the third configuration, the channel region is divided in to three. The potential distribution is mentioned in the following manner:

For the first and second configuration

$$\phi_i(x,y)=\phi_{si}(x)+a_{i1}(x)y+a_{i2}(x)y^2$$
$$0\le x\le L_i,0\le y\le t_{si} \tag{3}$$

where i=1,2

For the third configuration:

$$\phi_i(x,y)=\phi_{si}(x)+a_{i1}(x)y+a_{i2}(x)y^2$$
$$0\le x\le L_i,0\le y\le t_{si} \tag{4}$$

where i=1,2,3

The Poisson's equation is solved by using the following boundary conditions:

a) Electric flux at the front gate–oxide interface is continuous. For that reason, the following boundary is formed.

$$\left.\frac{\partial \phi_i(x,y)}{\partial y}\right|_{y=0}=\frac{C_{f,i}}{\varepsilon_{si}}(\phi_{si}(x)-V_{gsf,i}) \tag{5}$$

where is the ε_{si} is the dielectric constant of the silicon film and V_{gs} is the gate-source bias, $V_{gsf,i}$ is the gate-source voltage in the nanocavity (or) gate region, Φ_m,Φ_{si} are the work functions of the metal, silicon respectively.

Under nanocavity region,

$$V_{gsf,i}=V_{gsf}-\Phi_m-\Phi_{si}-\frac{qN_f}{C_{gap}} \tag{6}$$

$$C_{f,i}=\frac{\varepsilon_{bio}\varepsilon_{ox}}{\varepsilon_{bio}T_{ox}+\varepsilon_{ox}T_{bio}} \tag{7}$$

Under gate region,

$$V_{gsf,i}=V_{gsf}-\Phi_m-\Phi_{si} \tag{8}$$

$$C_{f,i}=\varepsilon_{ox}/t_{ox} \tag{9}$$

where $C_{f,i}$ is the capacitance of the nanocavity (or) gate region, N_f is the charge density of the biomolecules, $\varepsilon_{bio},T_{bio}$ are the dielectric constant of the biomolecules and thickness of nanocavity respectively. ε_{ox},t_{ox} are the dielectric constant and thickness of the gate oxide respectively. For the first configuration, region 1 (i=1) is assumed as a nanocavity region. For the second configuration, region 2 (i=2) is assumed as a nanocavity region. For the third configuration, region 1 and region 3 (i=1,3) are assumed as a nanocavity region.

b) Electric flux at the back gate–oxide and back channel interface is continuous,

c)

$$\left.\frac{\partial \phi_i(x,y)}{\partial y}\right|_{y=t_{si}}=\frac{C_{b,i}}{\varepsilon_{si}}(V_{gsb,i}-\phi_{bi}(x)) \tag{10}$$

where $\phi_{bi}(x)$ is the potential function along the back gate oxide–silicon interface of nanocavity (gate controlled) region. $C_{b,i}$ is the capacitance of the nanocavity region (gate controlled) at the back gate. As symmetrical biasing is assumed, $\phi_{bi}(x)$ equal to $\phi_{si}(x)$ and $V_{gsb,i}$ is equal to $V_{gsf,i}$. With the uniform gate materials in the front and back gate oxide made $C_{b,i}$ equals $C_{f,i}$.

d) Surface potential at the interface of the two dissimilar gate regions of the front gate is continuous,

For the first and second configurations,

$$\phi_{s1}(L_1)=\phi_{s2}(L_1) \tag{11}$$

For the third configurations,

$$\phi_{s1}(L_1) = \phi_{s2}(L_1) \tag{12}$$

$$\phi_{s2}(L_2) = \phi_{s3}(L_2) \tag{13}$$

e) Electric flux at the interface of two different regions of the front gate is continuous

For the first and second configurations,

$$\phi_{s1}'(L_1) = \phi_{s2}'(L_1) \tag{14}$$

For the third configurations,

$$\phi'_{s1}(L_1) = \phi'_{s2}(L_1) \tag{15}$$

$$\phi'_{s2}(L_2) = \phi'_{s3}(L_2) \tag{16}$$

The potential at the source end is

$$\phi_{s1}(0) = V_{bi} \tag{17}$$

where $V_{bi} = V_T \ln (N_A N_D/ni^2)$ is the built-in potential across the body-source junction and V_T is the thermal voltage, n_i is the intrinsic carrier concentration and N_A,N_D are the source/drain doping respectively.

f)The potential at the drain end is,

For the first and second configurations,

$$\phi_{s2}(L) = V_{bi} + V_{DS} \tag{18}$$

where V_{DS} is the applied drain-source bias. By applying the boundary conditions from (11) to (18) in the (2), (3) and (4), the constants are determined and written as follows,

$$a_{i1}(x) = \frac{C_{f,i}}{\varepsilon_{si}}(\phi_{si}(x) - V_{gsf,i}) \tag{19}$$

$$a_{i2}(x) = \frac{1}{2t_{si}\varepsilon_{si}}((C_{b,i}V_{gsb,i} + C_{f,i}V_{gsf,i}) - \phi_{si}(x)(C_{b,i} + C_{f,i})) \tag{20}$$

After substitution of constants in the Poisson's equation, the following second order partial differential equation is formed as a function of surface potential.

$$\phi_{si}''(x) - \phi_{si}(x)\left(\frac{C_{b,i} + C_{f,i}}{1 + \frac{C_{f,i}}{C_{si}} + \frac{C_{b,i} + C_{f,i}}{2C_{si}}}\right) = \frac{\frac{qN_A}{\varepsilon_{si}}}{1 + \frac{C_{f,i}}{C_{si}} + \frac{C_{b,i} + C_{f,i}}{2C_{si}}} - \frac{1}{C_{si}t_{si}^2}\frac{C_{b,i}V_{gsb,i} + C_{f,i}V_{gsf,i}}{1 + \frac{C_{f,i}}{C_{si}} + \frac{C_{b,i} + C_{f,i}}{2C_{si}}} \tag{21}$$

The roots of the second order equation has been found . As they are equal in magnitude and opposite in sign, the following exponential function is replaced in the surface potential expression.

For the first configuration,

$$\phi_{s1}(x) = A\exp(\sqrt{\alpha_1}x) + B\exp(-\sqrt{\alpha}_1 x) - \frac{\beta_1}{\alpha_1} \tag{22}$$

$$\phi_{s2}(x) = C\exp(\sqrt{\alpha_2}(x - L_1) + D\exp(-\sqrt{\alpha}_2(x - L_1)) - \frac{\beta_2}{\alpha_2} \tag{23}$$

For the second configuration,

$$\phi_{s1}(x) = C\exp(\sqrt{\alpha_2}x) + D\exp(-\sqrt{\alpha}_2 x) - \frac{\beta_2}{\alpha_2} \tag{24}$$

$$\phi_{s2}(x) = A\exp(\sqrt{\alpha_1}(x - L_1) + B\exp(-\sqrt{\alpha}_1(x - L_1)) - \frac{\beta_1}{\alpha_1} \tag{25}$$

$$\alpha_1 = \left(\frac{C_b' + C_f'}{1 + \frac{C_f'}{C_{si}} + \frac{C_b' + C_f'}{2C_{si}}}\right) \tag{26}$$

$$\beta_1 = \frac{\frac{qN_A}{\varepsilon_{si}}}{1 + \frac{C_f'}{C_{si}} + \frac{C_b' + C_f'}{2C_{si}}} - \frac{1}{C_{si}t_{si}^2}\frac{C_b'V_{gsb}' + C_f'V_{gsf}'}{1 + \frac{C_f'}{C_{si}} + \frac{C_b' + C_f'}{2C_{si}}} \tag{27}$$

$$\alpha_2 = \left(\frac{C_b + C_f}{1 + \frac{C_f}{C_{si}} + \frac{C_b + C_f}{2C_{si}}}\right) \tag{28}$$

$$\beta_2 = \frac{\frac{qN_A}{\varepsilon_{si}}}{1 + \frac{C_f}{C_{si}} + \frac{C_b + C_f}{2C_{si}}} - \frac{1}{C_{si}t_{si}^2}\frac{C_bV_{gsb} + C_fV_{gsf}}{1 + \frac{C_f}{C_{si}} + \frac{C_b + C_f}{2C_{si}}} \tag{29}$$

The boundary conditions (e) and (f) are useful in determining the constant values. The constant values in the two regions are expressed as,

$$D = \frac{a_2SP + a_2SQ + a_3P + a_3Q + a_4RQ - a_4RP - 2a_1QSP}{(1-R)S(-P-Q) + (1+R)t(P+Q) - 2RP(S+t)} \tag{30}$$

$$C = \frac{1}{S}\left[-Dt + V_{b1} + V_{DS}\right] \tag{31}$$

$$A = \frac{1}{2PS}\left[-D\left[-S + SR + t + tR\right] + a_2S + (1+R)a_4\right] \tag{32}$$

$$B = V_{bi} + \frac{\beta_1}{\alpha_1} - A \tag{33}$$

where , $P = e^{\sqrt{\alpha_1}L_1}$, $Q = e^{-\sqrt{\alpha_1}L_1}$, $R = \sqrt{\frac{\alpha_2}{\alpha_1}}$, $S = e^{\sqrt{\alpha_2}(L-L_1)}$, $t = e^{-\sqrt{\alpha_2}(L-L_1)}$, $a_1 = \frac{\beta_1}{\alpha_1}$ $a_2 = \frac{\beta_2}{\alpha_2}$, $a_4 = V_{bi} + V_{DS}$

For the third configuration,

$$\phi_{s1}(x) = A\exp(\sqrt{\alpha_1}x) + B\exp(-\sqrt{\alpha}_1 x) - \frac{\beta_1}{\alpha_1} \tag{34}$$

$$\phi_{s2}(x) = C\exp(\sqrt{\alpha_2}(x-L_1)) + D\exp(-\sqrt{\alpha}_2(x-L_1)) - \frac{\beta_2}{\alpha_2} \tag{35}$$

$$\phi_{s3}(x) = E\exp(\sqrt{\alpha_3}(x-L_2)) + F\exp(-\sqrt{\alpha_3}(x-L_2)) - \frac{\beta_3}{\alpha_3} \tag{36}$$

where,

$$\alpha_i = \left(\frac{C_{b,i} + C_{f,i}}{1 + \frac{C_{f,i}}{C_{si}} + \frac{C_{b,i} + C_{f,i}}{2C_{si}}} \right) \tag{37}$$

$$\beta_i = \frac{\frac{qN_A}{\varepsilon_{si}}}{1 + \frac{C_{f,i}}{C_{si}} + \frac{C_{b,i} + C_{f,i}}{2C_{si}}} - \frac{1}{C_{si}t_{si}^{\ 2}} \frac{C_{b,i}V_{gsb,i} + C_{f,i}V_{gsf,i}}{1 + \frac{C_{f,i}}{C_{si}} + \frac{C_{b,i} + C_{f,i}}{2C_{si}}} \tag{38}$$

where $C_{b,i}$,$C_{f,i}$,$V_{gsb,i}$,$V_{gsf,i}$ are shown in the equations (6) to (9). The boundary conditions (e) and (f) are useful in determining the constant values. The constant values in the three regions are expressed as,

$$A = \frac{\sqrt{\alpha_i\alpha_2}(a_1P - 4R) - P\alpha_1\alpha_2 + R(\sqrt{\alpha_1} + \sqrt{\alpha_2})}{-4\sqrt{\alpha_i\alpha_2} - (\sqrt{\alpha_1} + \sqrt{\alpha_2})(a_1^{\ 2}\alpha_2 - a_1^{\ 2}\alpha_1 - \alpha_2 - \alpha_1)} \tag{39}$$

$$D = \frac{-\sqrt{\alpha_1}(a_1P - 2R) + 2\sqrt{\alpha_1}A}{\sqrt{\alpha_1}a_1 + \sqrt{\alpha_2}a_1} \tag{40}$$

$$B = R - A \tag{41}$$

$$C = \frac{1}{a_1}\left[Pa_1 - R - (a_1^{\ 2} - 1)A + Da_1\right] \tag{42}$$

$$E = \frac{1}{2b_1\sqrt{\alpha_3}}\left[\begin{matrix} Qb_1\sqrt{\alpha_3} - \\ Cb_1^{\ 2}\left(\sqrt{\alpha_2} + \sqrt{\alpha_3}\right) + D\left(\sqrt{\alpha_2} + \sqrt{\alpha_3}\right) \end{matrix}\right] \tag{43}$$

$$F = \frac{1}{2b_1\sqrt{\alpha_3}}\left[\begin{matrix} -Qb_1\sqrt{\alpha_3} - \\ Cb_1^{\ 2}\left(\sqrt{\alpha_3} - \sqrt{\alpha_2}\right) + \\ D\left(\sqrt{\alpha_2} - \sqrt{\alpha_3}\right) \end{matrix}\right] \tag{44}$$

where,

$$P = \frac{\beta_1\alpha_2 - \beta_2\alpha_1}{\alpha_1\alpha_2}, \quad Q = \frac{\beta_2\alpha_3 - \beta_3\alpha_2}{\alpha_2\alpha_3}, \quad R = \frac{\beta_1}{\alpha_1} + V_{bi}, \quad S = \frac{\beta_3}{\alpha_3} + V_{bi} + V_{gs}$$

$$a_1 = e^{\sqrt{\alpha_1}L_1}, b_1 = e^{\sqrt{\alpha_2}L_2}, c_1 = e^{\sqrt{\alpha_2}(L_2 - L_1)}, d_1 = e^{\sqrt{\alpha_3}(L - L_2)}$$

5. Electric field

The electric-field distribution along the channel length can be determined by differentiating the surface potential and the Electric field can be written as,

For the first configuration,

$$E_1 = \left.\frac{d\phi_{s1}(x,y)}{dx}\right|_{y=0} = A\sqrt{\alpha_1}\exp(\sqrt{\alpha_1}x) - B\sqrt{\alpha_1}\exp(-\sqrt{\alpha}_1 x) \tag{45}$$

$$E_2 = \left.\frac{d\phi_{s2}(x,y)}{dx}\right|_{y=0} = C\sqrt{\alpha_2}\exp(\sqrt{\alpha_2}(x-L_1)) - D\sqrt{\alpha_2}\exp(-\sqrt{\alpha}_2(x-L_1)) \tag{46}$$

For the second configuration,

$$E_1 = \left.\frac{d\phi_{s1}(x,y)}{dx}\right|_{y=0} = C\sqrt{\alpha_2}\exp(\sqrt{\alpha_2}(x-L_1)) - D\sqrt{\alpha_2}\exp(-\sqrt{\alpha}_2(x-L_1)) \tag{47}$$

$$E_2 = \left.\frac{d\phi_{s2}(x,y)}{dx}\right|_{y=0} = A\sqrt{\alpha_1}\exp(\sqrt{\alpha_1}x) - B\sqrt{\alpha_1}\exp(-\sqrt{\alpha}_1 x) \tag{48}$$

For the third configuration,

$$E_1 = \left.\frac{d\phi_{s1}(x,y)}{dx}\right|_{y=0} = A\sqrt{\alpha_1}\exp(\sqrt{\alpha_1}x) - B\sqrt{\alpha_1}\exp(-\sqrt{\alpha}_1 x) \tag{49}$$

$$E_2 = \left.\frac{d\phi_{s2}(x,y)}{dx}\right|_{y=0} = C\sqrt{\alpha_2}\exp(\sqrt{\alpha_2}(x-L_1)) - D\sqrt{\alpha_2}\exp(-\sqrt{\alpha}_2(x-L_1)) \tag{50}$$

$$E_3 = \left.\frac{d\phi_{s3}(x,y)}{dx}\right|_{y=0} = E\sqrt{\alpha_3}\exp(\sqrt{\alpha_3}(x-L_2)) - F\sqrt{\alpha_3}\exp(-\sqrt{\alpha}_2(x-L_2)) \tag{51}$$

6. Threshold voltage

The threshold voltage is defined as the minimum voltage applied between gate and source in order to turn the device on. In order to derive the threshold voltage, the minimum surface potential approach is used. The minimum surface potential is derived for the two regions. Also, the obtained minimum potential is equated to twice of bulk fermi potential which is needed to invert the channel depends upon the substrate doping.

For the first configuration, the threshold voltage in the region 1 and 2 are written as

$$V_{threshold,1} = \left[-\alpha_1 \left(\frac{B^2}{2A} + \frac{B}{2} - 2\phi_F \right) + \frac{qN_A}{\varepsilon_{si}} \right] \frac{C_{si} t_{si}^{\ 2}}{2C_{f,1}} \quad (52)$$

$$V_{threshold,2} = \left[-\alpha_2 \left(\frac{D^2}{2C} + \frac{D}{2} - 2\phi_F \right) + \frac{qN_A}{\varepsilon_{si}} \right] \frac{C_{si} t_{si}^{\ 2}}{2C_{f,2}} \quad (53)$$

The minimum of (52) and (53) is considered as a threshold voltage of the DG MOSFET based biosensor.

For the second configuration, the threshold voltage in the region 1 and region 2 are written as,

$$V_{threshold,1} = \left[-\alpha_2 \left(\frac{D^2}{2C} + \frac{D}{2} - 2\phi_F \right) + \frac{qN_A}{\varepsilon_{si}} \right] \frac{C_{si} t_{si}^{\ 2}}{2C_{f,2}} \quad (54)$$

$$V_{threshold,2} = \left[-\alpha_1 \left(\frac{B^2}{2A} + \frac{B}{2} - 2\phi_F \right) + \frac{qN_A}{\varepsilon_{si}} \right] \frac{C_{si} t_{si}^{\ 2}}{2C_{f,1}} \quad (55)$$

The minimum of (54) and (55) is considered as a threshold voltage of the DG MOSFET based biosensor.

For the third configuration , the threshold voltage in the region 1,2 and 3 are written as,

$$V_{threshold,1} = \left[-\alpha_1 \left(\frac{B^2}{2A} + \frac{B}{2} - 2\phi_F \right) + \frac{qN_A}{\varepsilon_{si}} \right] \frac{C_{si} t_{si}^{\ 2}}{2C_{f,1}} \quad (56)$$

$$V_{threshold,2} = \left[-\alpha_2 \left(\frac{D^2}{2C} + \frac{D}{2} - 2\phi_F \right) + \frac{qN_A}{\varepsilon_{si}} \right] \frac{C_{si} t_{si}^{\ 2}}{2C_{f,2}} \quad (57)$$

$$V_{threshold,3} = \left[-\alpha_3 \left(\frac{F^2}{2E} + \frac{F}{2} - 2\phi_F \right) + \frac{qN_A}{\varepsilon_{si}} \right] \frac{C_{si} t_{si}^{\ 2}}{2C_{f,3}} \quad (58)$$

The minimum of (56) ,(57) and (58) is considered as a threshold voltage of the DG MOSFET based biosensor.

7. Sensitivity

The sensitivity in particular is defined as the relative variation in sensor characteristics when target molecules attach in the nanogap region. The change in threshold voltage before and after biomolecules' immobilization is considered as a sensing metric parameter and is defined as,

Sensitivity of a Biosensor when Neutral Molecules immobilized is mentioned as follows:

$$\Delta S = V_{threshold}\big|_{K=1} - V_{threshold}\big|_{K>1} \quad (59)$$

Sensitivity of a Biosensor when Charged Molecules immobilized is mentioned as follows,

$$\Delta S = V_{threshold}\big|_{N_f=0} - V_{threshold}\big|_{N_f\neq 0} \quad (60)$$

8. Results and discussion

The surface potential, Electric Field, threshold voltage and sensitivity of the various configurations of DG MOSFET based biosensor has been calculated and plotted. Also, the better performing structure is identified. The results are analyzed by varying the channel length, nanocavity thickness ,gate length ratios. Typical dimensions used for the DG MOSFET based biosensor structures are summarized in Table 1.

Table. 1. Typical dimensions used for DG MOSFET based biosensor structures

Parameter	Value
Thickness of the front gate oxide tf	2 nm
Thickness of the back gate oxide tb	2 nm
Thickness of the channel tsi	12 nm
Length of the Channel L	100 nm
Length of the nanocavity Lnano	10 nm- 50 nm
Thickness of the nanocavity Tnano	10 nm - 25 nm
Source/Drain Doping NA	10^{15} cm-3
Body Doping ND	$5x10^{19}$ cm-3
Gate Work Function	5.25 eV
Charge of biomolecule Nf	$-10x10^{16}$ - $+10x10^{16}$ C/m^2
Dielectric constant of biomolecule K	2-12

8.1. Surface potential

8.1.1. Comparison of surface potential

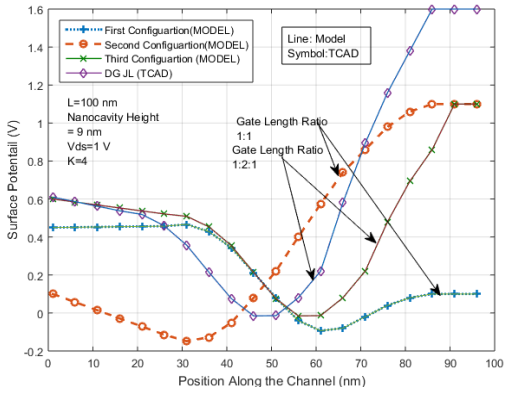

Fig. 4. Variation of Surface potential versus channel length for various DG MOSFET based biosensor configurations

In Fig. 4, the Surface potential profile results obtained from the analytical model are shown for the three different configuration of a DG-MOSFET based biosensor and the simulated model of a Junction less DG MOSFET based biosensor are shown. In Ajay et al. model (2015) [19], the DG JL MOSFET is deployed. This has a higher mobility than the classical transistors. So the potential at the drain end is comparatively higher. The device simulator TCAD is used to verify the proposed model of various configurations of DG MOSFET based biosensors. The model has very small deviation with the simulation results. It is clearly seen that the surface potential of the first configuration is stepping down function as biomolecules under the region 1 of the is modulating the work function. As a result of this, the first configuration is essentially screened from drain-potential variations. The second configuration it is a step up function, the biomolecules under region 2 of the gate is modulating the work function and the potential variation at the drain end is higher. This is due to the immobilization of biomolecules near the drain region. This second structure is encouraging the drain conductance. Here, the drain potential has been majorly influenced by biomolecules characteristics. At this the point at which the gate looses it's control. In the third configuration, the surface potential is a combination of decaying and rising exponential function. The dielectric modulation effect is predominant in this structure because of the presence of biomolecules is accomplished in both ends of the channel. Even though the electrostatic integrity is a major issue, in bio sensor modeling the influence of biomolecules in the electrical parameters of the device is expected to be maximum to model a high sensitive biosensor.

8.1.2. Immobilization of neutral biomolecules

The surface potential of DG MOSFET based biosensors for three different configurations have been plotted versus channel length is plotted in Fig. 5 In the view of short channel immunity, the first configuration is found to be more rigid to the drain conductance, thereby it is considered to be the suitable device structure to overcome DIBL effects. But the application of MOSFET as a biosensor exploits the property of the MOSFET that gives the measurable variation of device parameters when the biomolecules are applied in the nanoembedded cavity. If the neutral biomolecules is applied in the uncovered cavity, the gate capacitance is altered with respect to the dielectric constants of the biomolecules. This dielectric modulation effect is clearly visualized in the complete channel region of third configuration. In the first two configurations, the changes in the surface potential is microscopic. If the dielectric constant of a nanocavity region is varied from 4 to 8, the potential is altered by a factor of 11 for the third configuration. For the first, second configurations, it is altered by a factor of 9 and 0.5 respectively. Since the change is found appreciable in the third device structure, it is suggested to be the best fit device configuration for biosensing application.

8.1.3. Immobilization of charged biomolecules

Fig. 6 shows the variation of the surface potential versus the channel length. The drain conductance is dominant in the third and second structures as the drain end potential is controlled by the biomolecules effect not by the gate alone. Although the first configuration is mitigating DIBL effects, the impact of biomolecule in the channel region is unobservable. The second and third configuration shows the variation of surface potential is approximately about 6% and 3% respectively due to the charged biomolecues.

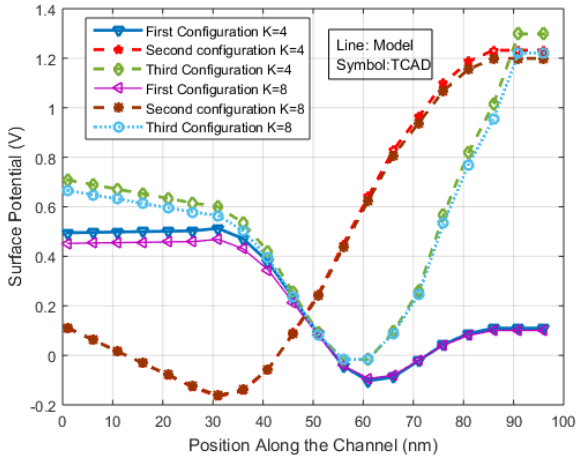

Fig. 5. Variation of surface potential versus channel length for various DG MOSFET based biosensor configurations with the neutral biomolecules

With the positively charged molecules, the device turn on with lesser threshold voltage when compared to negatively charged molecules. As a result, the potential when the nanocavity is filled with positive charged biomolecules are substantially greater.

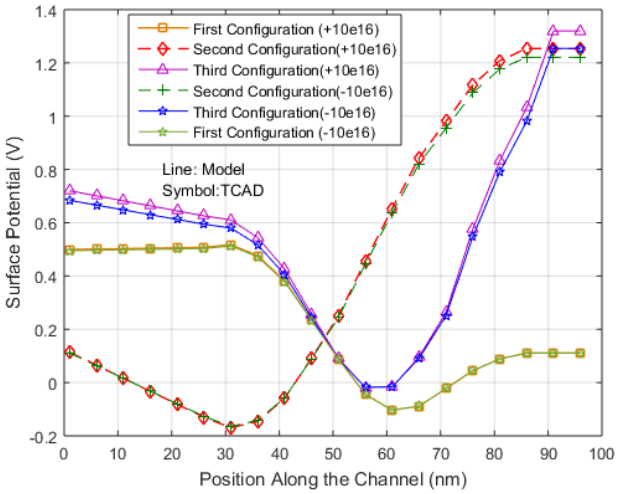

Fig. 6. Variation of surface potential versus channel length for various DG MOSFET based biosensor configurations with the charged biomolecules

8.2. Electric field

8.2.1. Comparison of electric field

Fig. 7 shows the calculated and simulated values of the electric field near the drain end for the three different configurations and the simulated values for the Venkateshwar Reddy and Jagadesh kumar model [20]. This model is taken for comparison as this model emphasize two different gate materials at the front gate, and because of the discontinuity of two materials the peak electric field of this model is reduced substantially. In the third configuration, the peak electric field is reduced by 20% approximately. All the configurations ensure a reduced hot carrier effect due to the discontinuity of the gate material. Also the results are verified with the TCAD simulation results.

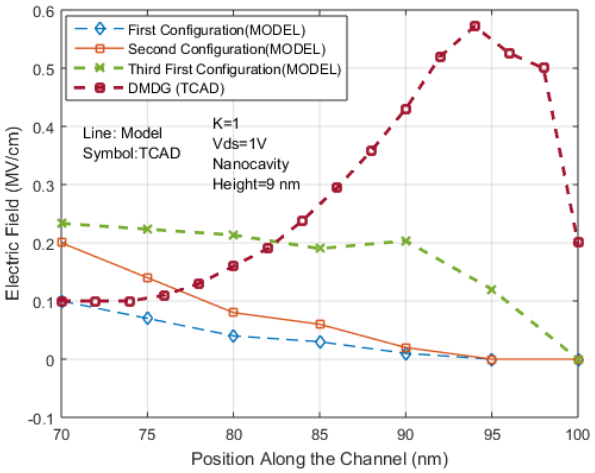

Fig. 7. Variation of Electric Field versus channel length for various DG MOSFET based biosensor configurations

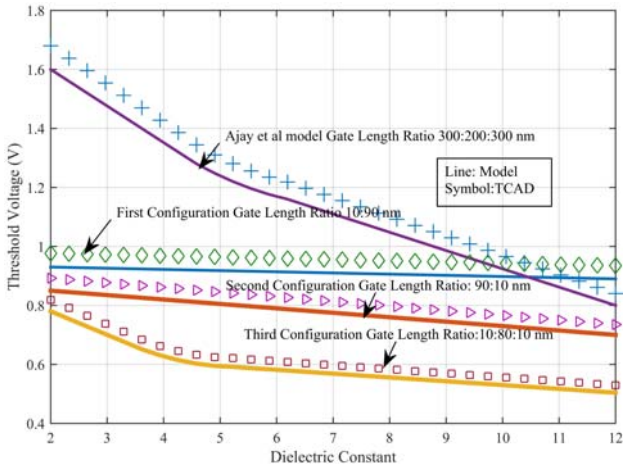

Fig. 8. Variation of threshold voltage for the neutral biomolecules with different dielectric constants for various configurations of DG MOSFET based biosensor with the gate length ratios 1:8:1 1nd 1:9

8.3. Threshold voltage

8.3.1. Impact of nanocavity length and the immobilization of charged biomolecules

Fig. 8 and Fig. 9. illustrate the threshold voltage variations for different dielectric constants. The dimension of the nanocavity is playing a vital role in threshold voltage variation. This analytical calculated model and it's simulation are compared with Ajay et al (2015) model which explains the Four split Gate MOSFET based biosensor [21].

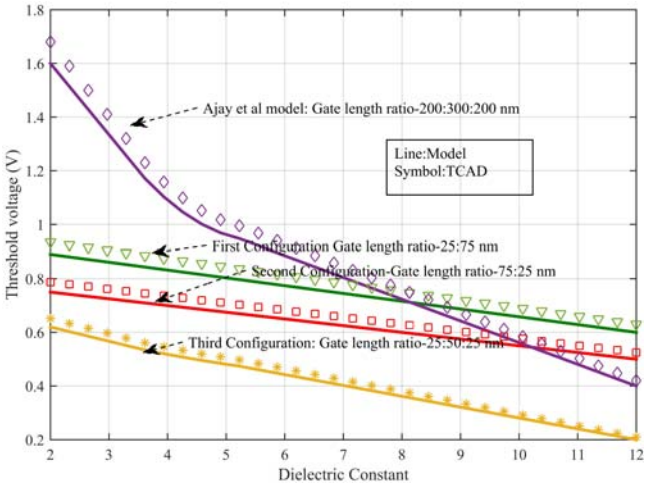

Fig. 9.Variation of threshold voltage for the neutral biomolecules with different dielectric constants for various configurations of DG MOSFET based biosensor with gate length ratio 1:1 and 1:2:1

In Fig. 8, the nanocavity length is kept small As in the four split gate model the uncovered region is. This assumption is indirectly assuming that only the small amount of biomolecules are placed in the nanocavity region. Because of the lesser influence of biomolecules , the threshold voltage of all the three configurations are affected less. In Fig.9,the nanocavity length is kept larger. This assumption is indirectly assuming that large amount of biomolecules are placed in the nanocavity region. Because of the higher influence of biomolecules , the threshold voltage of all the three configurations are affected little bit higher after a certain dielectric constant value. Before biomolecules immobilization, the cavity is assumed to be filled with air (Dielectric constant one). The different dielectric constant of a nanocavity region is varied from 2 to 11 in order to realize the neutral biomolecules. The change in the threshold voltage is observable when the dimension of nano cavity is kept as 50x9 nm for the first two configurations. The threshold voltage is a following a strong decaying relation when the nano cavity is 25x9 nm in both the sides instead of 10x9 nm.

8.3.2. Impact of nanocavity length and the immobilization of charged biomolecules

Fig. 10 and Fig. 11 demonstrate the threshold voltage variations for different charge density of biomolecules. This result has a major impact with the nanocavity dimension. The negatively charged biomolecules increase the threshold voltage and positive charges decrease the threshold voltage.

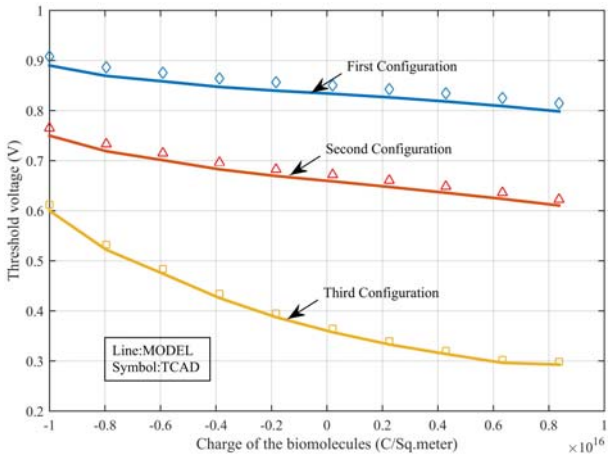

Fig. 10.Variation of threshold voltage for the charged biomolecules with positive and negative charges for various configurations of DG MOSFET based biosensor with gate length ratio 1:9 and 1:8:1

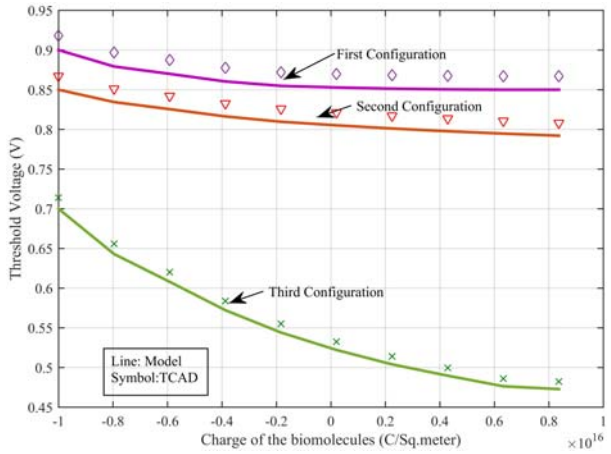

Fig. 11.Variation of threshold voltage for the charged biomolecule with positive and negative charges for various configurations of DG MOSFET based biosensor with gate length ratio 1:1 and 1:2:1

This is because of the relation between the threshold voltage and the charge density $(V_{tthreshold} \propto \frac{qN_f}{C_{gap}})$. Also the capacitance of the cavity $C_{gap} = \frac{\varepsilon_{bio}}{T_{cavity}}$, where ε_{bio} is the dielectric constant of a biomolecule and T_{cavity} is the thickness of the nanocavity. From this it should be noted that the thickness of the cavity is dictating a major role in the threshold voltage modeling. When the height of the cavity is increased, the variation in threshold voltage is clearly visible for the charged biomolecules.

8.4. Sensitivity

8.4.1. Comparison with the existing model

Fig. 12 shows the variation of sensitivity of the neutral biomolecules versus dielectric constant. This model is compared with the four gate MOSFET based long channel biosensor model. Also, the proposed model is compared with the TCAD simulation results for validation and the match is found good. The long channel model is having a high turn on voltage than our model. All the three configurations are showing the slightly increasing sensitivity with respect to the dielectric constant of a neutral biomolecules. The slope of the long channel biosensor's sensitivity line is about 25mV. For the proposed first configuration, the slope is approximately zero for a smaller cavity length. For the proposed second configuration, the slope is about 8 mV. For the proposed third configuration, the slope is about 50 mV. From this it may be justifiable that the third configuration with smaller cavity length is suggested as a suitable device for biosensing.

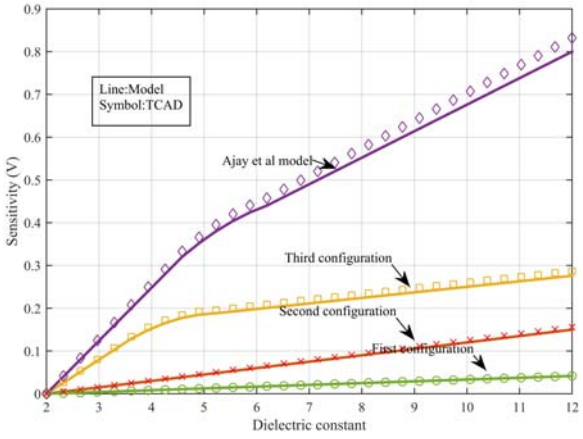

Fig.12.Variation of sensitivity for the neutral biomolecules with different dielectric constants for various configurations of DG MOSFET based biosensor with the smaller cavity length

8.4.2. Impact of nanocavity Length and the immobilization of neutral biomolecules

Fig. 13 shows the variation of sensitivity of the neutral biomolecules versus dielectric constant for two different cavity length. The dimension of the nano cavity is the most important affecting parameter in the biosensor modeling. The slope of the sensitivity line for a lengthy nano cavity is higher as the biomolecules impact on the device performance is more. For the second configuration ,

the slope of the nano cavity is invariantly 25 mV irrespective of the cavity length. For a third configuration the slope is calculated as 140mV, which dictates a exponential increment in the sensitivity parameter. From this ,the neutral biomolecules detection with higher sensitivity and with very few biomoleules is possible in a third configuration biosensor.

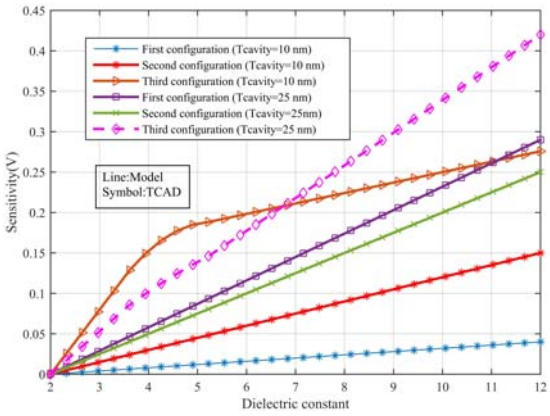

Fig. 13.Variation of sensitivity for the neutral biomolecules with different dielectric constants for various configurations of DG MOSFET based biosensor by varying cavity length

8.4.3. Impact of nanocavity Length and the immobilization of charged biomolecules

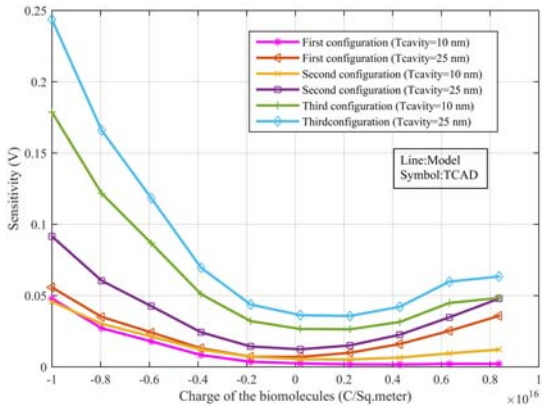

Fig. 14.Variation of absolute sensitivity for the charged for various configurations of DG MOSFET based biosensor by varying cavity length

From Fig. 14, the absolute value of sensitivity versus the charge of biomolecules is shown for a different cavity length. The sensitivity of the third configuration is better when compared to the other two configurations. The third configuration is producing a higher sensitivity even with smaller amount of biomolecules. The proposed model is governed by the negative biomolecules. The sensitivity is almost invariable with the positive biomolecules. Also, Fig. 14 emphasizes the importance of cavity dimension.

From Fig. 15, the sensitivity versus the charge of biomolecules is shown for a different cavity length. In all the configurations, sensitivity is increasing while the charge of biomolecule is increased. This increment is linear for a negatively charged biomolecules sand saturated for the positively charged biomolecules. This is because of the rate of change of the threshold voltage is mostly affected by the negatively charged biomolecules. It is noticeable that the calculated sensitivity for the third configuration is the highest.

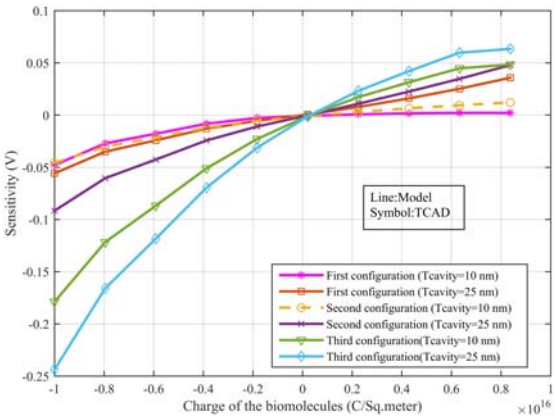

Fig. 15.Variation of sensitivity for the charged for various configurations of DG MOSFET based biosensor by varying cavity length

9. Conclusion

In this paper, the sensitivity of the three different configurations have been modeled and the results are validated with TCAD results. Also, the results are compared with the previous work results. The impact of charged and neutral biomolecules in the device parameters like surface potential, Threshold voltage and Sensitivity are analytically modeled and discussed. The immunity against the SCEs of three configurations are discussed. Even though the superior device structure is identified to mitigate SCEs, the suitability is justified with respect to the requirement of a biosensor.

From this detailed analysis it should be noted that the impact of the location of target molecules (position of the nanocavity) and the quantity of the biomolecules (height of the nanocavity) on the performance metric parameter such as sensitivity is clearly discussed. Among three configurations, the third configuration is having better sensitivity with the smaller cavity and small amount of detection samples. Hence, for a cost-effective biomedical diagnosis , the third configuration is considered as a proper choice.

Acknowledgements

The authors would like to thank all the team members of the National Instruments Electronics System Design (ESD) Laboratory, Thiagarajar College of Engineering (TCE), Tamil Nadu, India for their technical advice and direct and indirect contributions.

References

[1] Schaller, R. Robert, IEEE Spectrum **34** (6), 52 (1997).
[2] Manoj Kumar, Subhasis Haldar, Mridula Gupta, Radhey, S. Gupta, Nanomaterials and Energy **5**(1), 10 (2016).
[3] R. Narang, K. S. Reddy, M. Saxena, R. S. Gupta, M. Gupta, IEEE T. Electron. Dev. **59**(10), 2809 (2012).
[4] R. Narang, K. S. Reddy, M. Saxena, R. S. Gupta, M. Gupta, IEEE Electron Device L **33**(2), 266 (2012).
[5]R. Narang, M. Saxena, M. Gupta, Superlattice Microst. **85**, 557 (2015).
[6]A. S.Chakraborty,S. Mahapatra, IEEE T Electron. Dev. **64**(4), 1519 (2017).
[7]P. Bergveld, Biosensors **2**(1), 15 (1986).
[8]D. Sarkar, W. Liu, X. Xie, A. C.Anselmo, S. Mitragotri, K. Banerjee, ACS Nano. **8**(4), 3992 (2014).
[9]D.Vasileska, D. K.Schroder, D. K. Ferry, IEEE T Electron. Dev. **44**(4), 584 (1997).
[10] P. Vimala, N. B. Balamurugan, N. B., International Journal of Electronics **100**(9), 1283 (2013).
[11] J. T. Park, J. P. Colinge, IEEE T Electron. Dev. **49**(12), 2222 (2002).
[12] J. P. Colinge, J. Inf. Sci. Technol. **11**(1), 3 (2008).
[13] S. Caras, J. Janata, Analytical Chemistry. **52**(12), 1935 (1980).
[14] S. H. Han, S. K. Kim, K. Park, S. Y. Yi, H. Park, H. Lyu, M. Kim, B. H. Chung, Anal. Chim. Acta **665**(1), 79 (2010).
[15] E. Souteyrand, J. Cloarec, J. Martin, C. Wilson, I. Lawrence, S. Mikkelsen, M. Lawrence, J. Phys.Chem. B **101**(15), 2980 (1997).
[16] M. Kaisti, Biosensors and Bioelectronics **98**, 437 (2017).
[17] Y. Chen, R. Ren, H. Pu, X. Guo, J. Chang, G. Zhou, S. Mao, M. Kron, J. Chen, Scientific Reports **7**(1), 10974 (2017).
[18] G. P. Beyer, C. W. Scarantino, B. R. Prestidge, A. G. Sadeghi, M. S. Anscher, M. Miften, T. B. Carrea, M. Sims, R. D. Black, International Journal of Radiation Oncology Biology Physics **69**(3), 925 (2007).
[19] Ajay, Rakhi Narang, Manoj Saxena, Mridula Gupta, Superlattice Microst. **85**, 557 (2015).
[20] G. Venkateshwar Reddy, M. Jagadesh Kumar, IEEE T Nanotechnol. **4**(2), 260 (2005).
[21] Ajay, Rakhi Narang, Manoj Saxena, Mridula Gupta, IEEE T Electron. Dev. **62**(8), 2636 (2015).

*Corresponding author: buvaneswaricsk@gmail.com